Nanostructured sulfur cathodes†

Yuan Yang,[a] Guangyuan Zheng[b] and Yi Cui*[ac]

Rechargeable Li/S batteries have attracted significant attention lately due to their high specific energy and low cost. They are promising candidates for applications, including portable electronics, electric vehicles and grid-level energy storage. However, poor cycle life and low power capability are major technical obstacles. Various nanostructured sulfur cathodes have been developed to address these issues, as they provide greater resistance to pulverization, faster reaction kinetics and better trapping of soluble polysulfides. In this review, recent developments on nanostructured sulfur cathodes and mechanisms behind their operation are presented and discussed. Moreover, progress on novel characterization of sulfur cathodes is also summarized, as it has deepened the understanding of sulfur cathodes and will guide further rational design of sulfur electrodes.

1. Introduction

Rechargeable batteries with superior performance are desired to solve imminent energy and environmental issues.[1–3] State-of-the-art technologies, such as Li-ion batteries, dominate the portable electronics market but are not satisfactory for applications such as electric vehicles and grid-level energy storage due to their high cost and low energy density.[4,5] The demand for advanced batteries with high energy density, long cycle life and low cost drives the urgent search for new systems with superior performance over current technologies. The Li/S battery is an attractive and promising candidate among emerging battery technologies.[6]

The concept of utilizing elemental sulfur as a cathode electrode material was first introduced by Herbet and Ulam in 1962[7] and Argonne National Laboratory in 1967.[8] In a Li–S cell, the overall reaction during discharge can be described as

$$S_8 + 16Li^+ + 16e^- \rightarrow 8Li_2S \text{ (cathode)}$$

$$16Li \rightarrow 16Li^+ + 16e^- \text{ (anode)}$$
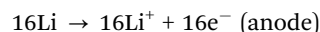
Sulfur and lithium have theoretical specific capacities of 1673 and 3861 mAh g^{-1}, respectively. The average voltage of the full cell is 2.15 V. This results in a theoretical energy density of 2500 Wh kg^{-1} or 2800 Wh L^{-1},[4,9] which is significantly higher than the current $LiMO_2$–graphite system (M = $Ni_{1/3}Mn_{1/3}Co_{1/3}$) and projected high-energy $LiMO_2$–silicon batteries (Fig. 1a).

[a] *Department of Materials Science and Engineering, Stanford University, Stanford, California 94305, USA. E-mail: yicui@stanford.edu*

[b] *Department of Chemical Engineering, Stanford University, Stanford, California 94305, USA*

[c] *SLAC National Accelerator Laboratory, Stanford Institute for Materials and Energy Sciences, 2575 Sand Hill Road, Menlo Park, California 94025, USA*

† Part of the chemistry of functional nanomaterials themed issue.

Dr Yuan Yang joined Prof. Yi Cui's group at Stanford University in 2007 and graduated with a PhD in Materials Science in 2012. Currently he is a postdoctoral researcher in the department of mechanical engineering at MIT. At Stanford, Dr Yang focuses on developing new materials, especially Li_2S and sulfur cathode for high energy rechargeable batteries. He also developed a transparent battery for electronics.

Yuan Yang

*Guangyuan Zheng is a PhD student in the Department of Chemical Engineering at Stanford University. He received his BA in Chemical Engineering from the University of Cambridge. He is a recipient of the National Science Scholarship from A*STAR in Singapore. Under the supervision of Prof Yi Cui, his research focuses on the development of nanostructured materials and renewable materials for energy applications.*
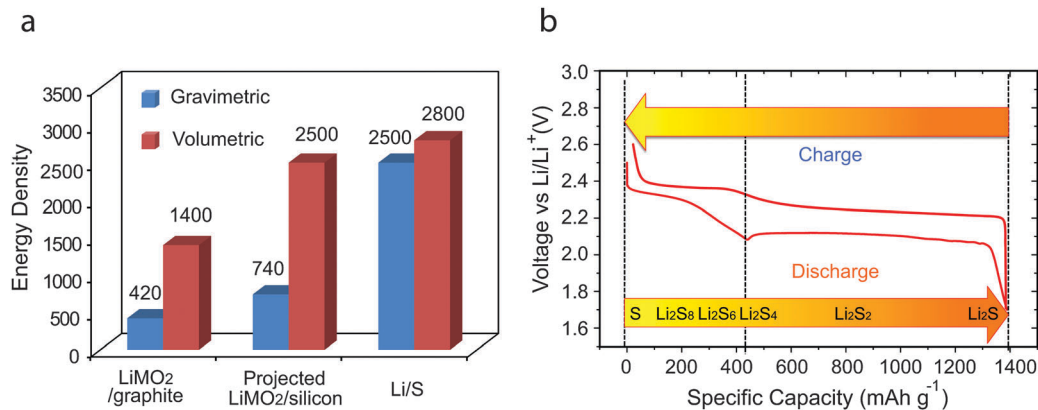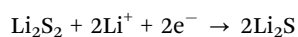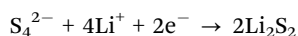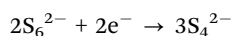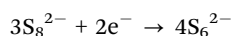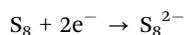
Guangyuan Zheng

a

b

Fig. 1 Introduction to the Li/S battery. (a) The theoretical energy density of different rechargeable battery systems based on active materials only. The units are Wh kg^{-1} and Wh L^{-1} for gravimetric and volumetric energy density, respectively. M = Ni$_{1/3}$Mn$_{1/3}$Co$_{1/3}$ for the LiMO$_2$–graphite system. For projected LiMO$_2$–silicon cell, the specific capacity for the cathode and anode are 250 and 3000 mAh g^{-1}, respectively. The density is 4.8 g cm^{-3} for LiMO$_2$, and the capacity per volume is 2200 mAh L^{-1} for silicon after considering the necessary space for volume expansion. (b) The voltage profile and chemistry of sulfur cathode in the organic electrolyte.

The common Li/S battery architecture is comprised of a positive electrode of sulfur, carbon additives and binder, and a metallic lithium anode separated by an organic electrolyte. In the organic liquid electrolyte, the discharge of the sulfur cell proceeds through multiple steps:[10,11]

$$S_8 + 2e^- \rightarrow S_8{}^{2-}$$

$$3S_8{}^{2-} + 2e^- \rightarrow 4S_6{}^{2-}$$

$$2S_6{}^{2-} + 2e^- \rightarrow 3S_4{}^{2-}$$

$$S_4{}^{2-} + 4Li^+ + 2e^- \rightarrow 2Li_2S_2$$

$$Li_2S_2 + 2Li^+ + 2e^- \rightarrow 2Li_2S$$

The first three steps correspond to the high plateau (2.15–2.4 V) in the voltage profile (Fig. 1b), and polysulfide species produced in these steps are soluble in the electrolyte. In the last two steps, insoluble Li$_2$S$_2$ and Li$_2$S are formed and they precipitate out at the cathode. The corresponding voltage is lower, as indicated by the long plateau at 2.1 V. The first four steps have fast or moderate kinetics, while the last step of converting Li$_2$S$_2$ to Li$_2$S is difficult and is impeded by slow solid-state diffusion. Consequently, the voltage drops rapidly once Li$_2$S covers the whole electrode framework, resulting in the termination of discharge. Fig. 1b shows a summary of the reaction sequence of the sulfur cathode and the corresponding electrochemical profile.

Although the Li/S battery has considerable advantages when considering the energy density and cost, there are many challenges associated with its commercialization. The first is related to the volume change of sulfur particles during charge and discharge. Sulfur has a density of 2.03 g cm^{-3}, while Li$_2$S is lighter (1.66 g cm^{-3}). As a result, the volume expansion when sulfur is fully converted to Li$_2$S is as large as 80%. This volume change leads to pulverization of active materials and thus fast capacity decay. Second, Li$_2$S is both electronically and ionically insulating. Stoichiometric Li$_2$S has an electronic resistivity greater than 10^{14} ohm cm, and the Li$^+$ diffusivity in Li$_2$S is as low as 10^{-15} cm^2 s^{-1}.[12] Once a thin Li$_2$S layer completely covers the whole electrode, further lithiation will be largely impeded and the voltage decreases rapidly. Consequently, complete conversion of sulfur to Li$_2$S is difficult and most reports show discharge capacity less than 80% of the theoretical limit. Third, polysulfides are soluble in the electrolyte. These soluble species can be reduced to Li$_2$S at the lithium anode surface, passivating the anode and leading to both material loss and an increase in impedance. Moreover, the dissolution and precipitation process alters the morphology of the cathode in each cycle, which induces strain inside the electrode and degrades the cycle life.[13] The dissolution of polysulfides also results in the so-called shuttle effect, where long chain polysulfides (LCPs) diffuse to the surface of the lithium anode and are reduced to

Yi Cui is an Associate Professor and David Filo and Jerry Yang Faculty Scholar in the Department of Materials Science and Engineering at Stanford University and SLAC National Accelerator Laboratory. His current research is on nanomaterials for energy storage, photovoltaics, topological insulators, biology and environment. He received his PhD in Chemistry from Harvard University and was a Miller Postdoctoral Fellow at the University

Yi Cui

of California, Berkeley. He is an Associate Editor of Nano Letters. He is a co-director of the Bay Area Photovoltaics Consortium. He has founded Amprius Inc., a company to commercialize the high energy battery technology. He has received the Wilson Prize (2011), the Sloan Research Fellowship (2010), and the Technology Review World Top Young Innovator Award (2004).

short chain polysulfides (SCPs). The SCPs can then move back to the cathode and be oxidized to LCPs. This parasitic process takes place continuously, creating an internal "shuttle" phenomenon. It decreases the active mass utilization in the discharge process and markedly reduces the Coulombic efficiency.[4,9,14] Besides challenges related to the sulfur cathode, the use of lithium metal anodes results in safety concerns and energy density penalties due to the use of excess lithium;[15,16] these concerns warrant careful examination in the future.

To solve these challenges, rational design of the electrode structure is necessary. Based on literature studies and our own research in the past several years, we believe that the ideal sulfur electrode structure should have the following characteristics:[17] (1) sufficient space to accommodate sulfur volumetric expansion; (2) small dimensions of the active material to avoid pulverization; (3) short transport pathways for both electrons and Li ions to achieve high capacity and high power capability; (4) a large conductive surface area for deposition of insulating Li_2S_2 and Li_2S in order to preserve the morphology of the electrode; (5) effective trapping of polysulfides through physical and chemical means, and finally (6) appropriate electrolyte additives to passivate the lithium surface to minimize the shuttle effect. Some of these characteristics require structural designs that are self-conflicting. For example, a large surface area for Li_2S_2 and Li_2S deposition is prone to result in an open structure and thus will lead to ineffective trapping of polysulfides. The difficulties associated with fulfilling all these requirements simultaneously explain why it is very challenging to realize sulfur electrodes with high specific capacity and long cycle life.

In the past five to ten years, tremendous progresses have been made in understanding and improving the performance of sulfur cathodes. Nanostructures have played an important role in the development, as they provide new merits and opportunities to design better electrodes. For example, nanostructures are beneficial for criteria 1–4 above, and criterion 5 could be satisfied through structural design, such as utilizing a core–shell structure and an inactive matrix. A summary of the issues associated with sulfur cathodes and the merits of employing nanostructures are listed in Table 1. In the following sections, various nanostructured sulfur cathodes will be presented. We will not only list reported results, but also describe the advantages and limits of each approach. In addition to nanostructures, other pathways for improvement, such as electrolyte additives and binder modification, are also addressed. After discussing how to improve the performance of sulfur cathodes, recent advances in characterizing sulfur cathodes will be presented. Nanocharacterization tools have greatly improved our understanding of sulfur electrodes and will help guide the future design of sulfur electrodes.

2. Nanostructured sulfur cathodes

The development of nanostructured sulfur cathodes can be divided into several categories based on the composition and structure of the electrodes: (1) nanoporous carbon–sulfur composites, (2) graphene–sulfur composites, (3) one dimensional (1D) carbon–sulfur composites, (4) conductive polymer–sulfur composites, (5) porous oxide additives, and (6) nanostructured Li_2S cathodes. The first three approaches use carbon as a conductive pathway and as a matrix to trap polysulfides. However, different carbon structures have their own advantages and limitations. The polymer–sulfur composite uses soft polymers instead of carbon, which are more flexible and may accommodate more strain. Porous oxides have recently been found to improve capacity retention in sulfur cathodes, albeit with limited understanding of the mechanisms involved. The Li_2S cathode is an emerging research area to explore; it can be paired with a lithium-free anode to avoid the safety concerns and low Coulombic efficiency of the lithium metal anode. Developments of novel electrolyte, electrolyte additives and binders will also be discussed at the end of this section, as they play an important role in enhancing the overall performance of Li–S batteries. The advances discussed here have dramatically improved the performance of sulfur cathodes and have broadened people's understanding of the system.

2.1 Porous carbon–sulfur composite

A nanoporous carbon–sulfur composite is a mixture of porous carbon and sulfur where sulfur mainly exists inside the carbon pores. The porous carbon matrix helps trap dissolved polysulfides and improves the electronic conductivity of the electrode composite. The nanopores also accommodate volume expansion and strain inside the structure if an empty pore space is included in the design. Early work in this area was performed by Wang et al.,[18,19] where activated carbon with a pore size of around 2.5 nm was used as the conductive matrix. A reversible capacity of 400 mAh g^{-1} was achieved. A hierarchical meso/microporous carbon matrix was also employed, resulting in high initial capacity.[20]

A quantum leap in this approach was the utilization of ordered CMK-3 mesoporous carbon to trap polysulfides, as reported by Ji et al.[21] CMK-3 carbon comprises an assembly of hollow 6.5 nm-thick carbon rods separated by empty 3–4 nm-wide channel voids.[22] The channel space is spanned by carbon microfibers that prevent the collapse of the nano-architecture of the two-dimensional hexagonally ordered carbon rods. The small pore size efficiently traps polysulfides and facilitates fast electronic and ionic transport (Fig. 2a). The intake of sulfur within the pores is accomplished by simply heating sulfur and

Table 1 Issues associated with sulfur cathodes and solutions afforded by nanostructures

| Issues of sulfur cathode	Merits of nanostructures
Volume expansion and pulverization of sulfur	Small size allows accommodation of strain without fracture
Low electrical conductivity and ionic diffusivity of Li_2S	Short distance for electronic and ionic transport Large surface area to deposit Li_2S
Polysulfide dissolution	Exotic and flexible designs
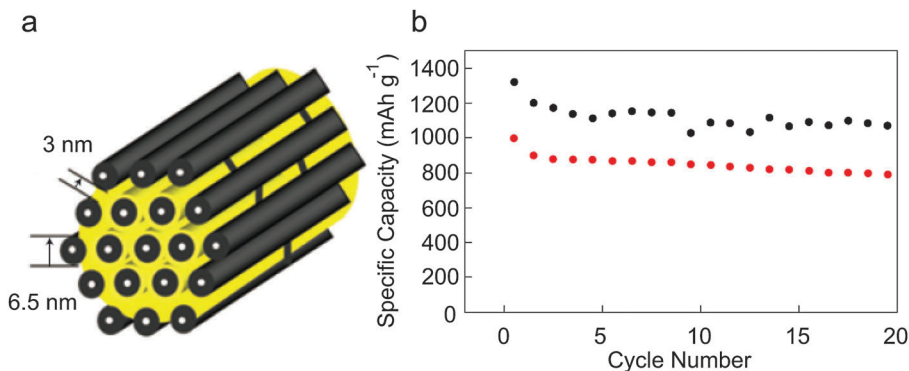
Fig. 2 (a) A schematic diagram of sulfur (yellow) confined within the interconnected pore structure of mesoporous carbon (CMK-3) formed from carbon tubes that are held together by carbon nanofibers. (b) Cycling performance of CMK-3/S modified with PEG (upper points, in black) *versus* CMK-3/S (lower points, in red) at a rate of 168 mA g^{-1} at room temperature.[21] The figure is reprinted with permission from ref. 21.

CMK-3 carbon together at 155 °C, where sulfur melts and has the lowest viscosity.[23] The amount of sulfur in the composite can be optimized to leave enough space for volume expansion. In the work of Ji *et al.*, the weight ratio of sulfur to CMK-3 carbon is 7 : 3. The mass of sulfur in the final electrode is ∼1.1 mg cm^{-2}, which accounts for 59% of the total weight of the electrode. This heating method has been widely adopted to incorporate sulfur into various carbon or polymer structures.[17,20,24–27] The CMK-3/ sulfur composite electrode was shown to exhibit a high initial discharge capacity of 1005 mAh g^{-1}, and it was improved to 1320 mAh g^{-1} by linking the carbon surface with polyethylene glycol (PEG) to further trap polysulfides (Fig. 2b). The specific capacity is based on the mass of sulfur. In this review, all specific capacity is based on the mass of sulfur unless specified. These values are much higher than earlier reports, indicating the importance of incorporating sulfur into pores within carbon nanostructures.

A porous hollow carbon sphere@sulfur composite has also been demonstrated to improve the cycle life.[28] The carbon sphere has a hollow core with a diameter of about 200 nm and a mesoporous carbon shell with a thickness of ∼40 nm. Sulfur is stored in the porous shell and can expand towards the inside of the sphere during lithiation. A discharge capacity of over 950 mAh g^{-1} was demonstrated with a capacity decay of only ∼10% per 100 cycles, which is among the best results of sulfur batteries.

The porous carbon matrix can significantly improve the cycle life of the sulfur cathode. However, the power capability at high sulfur content is still not satisfactory.[20,24,25] For example, an initial capacity of 1135 mAh g^{-1} was achieved at a 1 C rate with 40 wt% sulfur loading, but the capacity dropped to 718 mAh g^{-1} when the sulfur content was increased to 60 wt% in the composite.[24] To improve the power capability at high sulfur contents, a close-packed structure of bimodal porous carbon spheres was synthesized. In this composite, mesoporous carbon nanospheres with diameters of 300 ± 40 nm form an interconnected close-packed structure.[29] Two kinds of pores exist in the nanospheres with diameters of 6 nm and 3 nm. The relatively large space between nanospheres facilitates electrolyte infiltration, which leads to high power capability, and the small pores act as

reservoirs for sulfur storage. A capacity of 830 mAh g^{-1} was maintained after 100 cycles at a current rate of 1 C. The mass loading of sulfur is ∼0.8 mg cm^{-2}, accounting for 50–60% of the total weight. The authors also demonstrate that removal of sulfur from the surface of the carbon nanospheres and a thin SiO$_2$ coating help enhance the performance of the electrode. Removing sulfur on the surface minimizes the amount of sulfur that can readily dissolve into the electrolyte. These results demonstrate the importance of trapping sulfur inside carbon pores.

It is also noteworthy that pore size affects the voltage profile and electrochemistry of the sulfur cathode. Reports on mesoporous and macroporous carbon–sulfur composites show the typical two plateau behavior of the sulfur electrode.[20,21,24,29,30] In contrast, microporous carbon/sulfur composites have a good cycle life but a different voltage profile, with a significant capacity between 1.5 and 2 V *vs.* Li/Li$^+$.[25] Such a behavior is also observed in carbon/sulfur composites heated above 300 °C.[18,19,31] It is likely that sulfur is no longer in the S$_8$ cyclical structure in these composites; instead, sulfur and carbon may be mixed at the atomic level. Consequently, the corresponding Gibbs free energy of the reaction is different.

Nanoporous carbon–sulfur composites represent a clever method to improve the performance of the sulfur cathode, as shown in the examples above. To realize enhanced performance, the following aspects should be carefully considered: (1) optimized pore size and closed structure to trap polysulfides and minimize pulverization, (2) large pore volume to increase the content of sulfur for practical applications and (3) maximized amount of sulfur inside carbon pores.

2.2 Graphene (oxide)–sulfur composite

Graphene is made up of atomically thin planar sheets of carbon atoms that are packed in a honeycomb crystal lattice, giving the material high electrical conductivity.[32] Graphene oxide is oxidized graphene, where oxygen bonds to the lattice in forms such as –OH, C–O–C, and C═O. Graphene (oxide) has high surface area, chemical stability, and mechanical strength and flexibility, making it a useful growth substrate to anchor active materials for electrochemical energy storage applications.[33–39] The strong electronic coupling renders insulating active materials conducting, which

significantly increases the available specific capacity and rate capability of the composite electrode materials.[39,40] Graphene can either coat onto the surface of sulfur particles or form a sandwich-like composite to immobilize sulfur nanoparticles. Moreover, it is feasible to controllably functionalize the graphene surface with various groups, such as hydroxyl and carboxyl groups.[41,42] The functional groups could interact strongly with polysulfides to accomplish better trapping.

Early work on graphene (oxide)–sulfur composite materials produced by the mixing and heating method was reported by Wang et al.[43] However, the results suggested that this approach is not very effective in trapping polysulfides since the composite does not have a closed structure and polysulfides diffused out easily. Solution processing is a more effective method to form a uniform sulfur/graphene composite with a closed structure, as demonstrated by a number of groups.[40,44–47]

A graphene oxide-wrapped sulfur composite synthesized through solution processing was demonstrated by Wang et al. in 2011 (Fig. 3).[40] Sub-micron-sized sulfur particles were synthesized by reacting sodium thiosulfate with hydrochloric acid in an aqueous solution along with Triton X-100 surfactant, which was used as a capping agent to limit the size of the sulfur particles. During the synthesis, well-dispersed mildly oxidized graphene (mGO) solution was added to the reactor. Since the graphene oxide solution is not stable under acidic conditions, a layer of graphene oxide precipitates out and coats the sulfur particles. Carbon black was also added to the mGO solution to enhance the conductivity of the final product (Fig. 3). The as-synthesized sulfur particles are less than 1 μm in size, and the surface is coated with Triton X-100 and mGO in sequence. Advantages of this structure and the processing method are: (1) the graphene oxide and Triton X-100 surfactant can help trap the polysulfides as they form, (2) during expansion of sulfur, the graphene oxide layers can adjust their position and configuration to accommodate the volumetric strain, (3) the

carbon black additive and the mGO coating help improve the conductivity of the composite, and (4) the solution-based fabrication process is inexpensive and scalable. This rational approach leads to stable specific capacities of around 600 mAh g^{-1} and decay of only 10–15% per 100 cycles, which are promising characteristics for high-performance sulfur cathodes. The total mass loading of the electrode is 2–3 mg cm^{-2} and sulfur accounts for ~56% of the weight. However, the capacity of this electrode is not as high as the porous carbon–sulfur composite. A possible reason is that lithium ions cannot directly penetrate the hexagonal carbon lattice but need to find boundaries between mGO sheets to diffuse towards the sulfur particles, which impedes fast charge and discharge.

Sandwich-like graphene (oxide)–carbon composites have also been synthesized to enhance the performance.[44,45] For example, through a combination of solution synthesis and post-synthesis heat treatment, a thin sulfur layer with a thickness of tens of nanometers was homogenously dispersed between GO layers with a limited fraction of bulk sulfur exposed to the electrolyte.[45] Such a sandwich-like structure can accommodate the significant volume changes of sulfur upon cycling. Furthermore, the functional groups on GO have the ability to anchor sulfur atoms and effectively prevent the lithium polysulfides from dissolving into the electrolyte during cycling, which was confirmed by ab initio simulations and X-ray absorption spectroscopy. The as-fabricated sulfur cathode shows a high discharge capacity of 900 mAh g^{-1} with a sulfur content of 46.2 wt%, and there is no capacity decay in the first 50 cycles. The Coulombic efficiency is close to 100%. It should be noted that the ionic liquid electrolyte employed also plays a role in the good cycling performance, since the common poly(ethylene glycol) dimethyl ether (PEGDME) electrolyte results in worse cycling performance.

In general, graphene (oxide)–sulfur composites have similar advantages as other porous carbon–sulfur composites. Graphene (oxide) can also be functionalized to enhance its affinity for sulfur
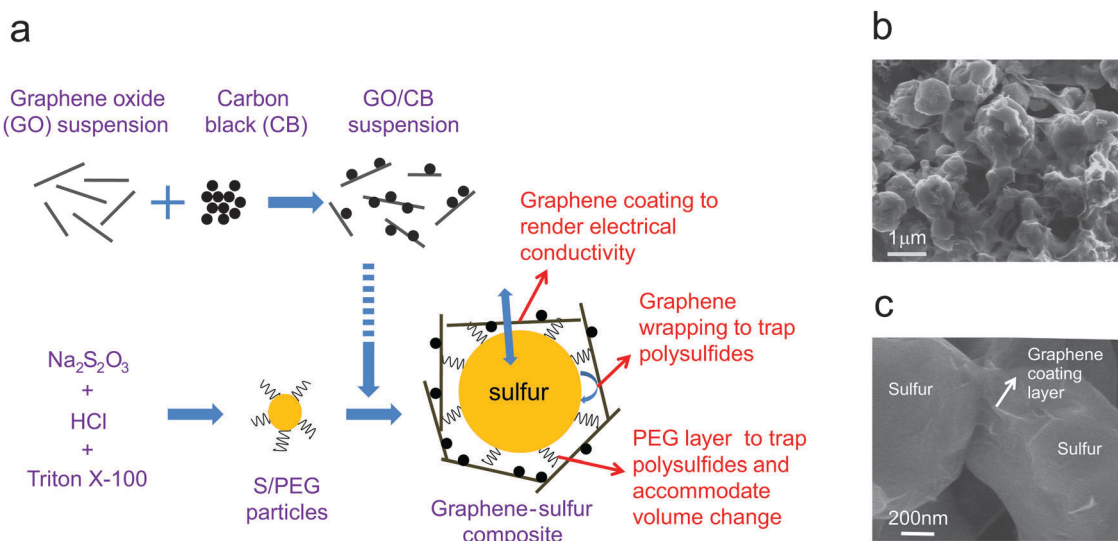

Fig. 3 (a) Schematic of the synthesis steps for a graphene–sulfur composite, along with a proposed schematic structure of the composite. (b and c) SEM characterization of the graphene–sulfur composite at low (b) and high (c) magnification.[40] The figure is reprinted with permission from ref. 40.

3022 | Chem. Soc. Rev., 2013, **42**, 3018–3032

This journal is © The Royal Society of Chemistry 2013

and polysulfides. In addition, the solution-based fabrication methods are more scalable than other options. However, possible limitations of using graphene (oxide) are that the graphene lattice could impede the transport of lithium ions and the conductivity of graphene oxide strongly depends on the degree of oxidation.

2.3   1-D carbon nanostructure/sulfur electrodes

In the conventional method of fabricating sulfur electrodes, elemental sulfur is normally mixed with some conductive matrix such as carbon black or conductive polymer and heated to obtain a composite structure. In these types of mixtures, residual sulfur particles with sizes in the range of microns usually remain within the electrode framework without being encapsulated in pores. Due to the significant morphological changes of sulfur during the charge–discharge process,[48] loss of electrical contact between the active material and the current collector can play a significant role in the initial capacity decay.[13] The reaction of sulfur with lithium normally involves a solid–liquid–solid process in which the dissolved polysulfides in the electrolyte react with lithium ions and then deposit on the conductive matrix as lithium sulfide. The formation of pores in the electrode and inhomogeneous precipitation of lithium sulfide can result in lower active material utilization as cycling proceeds. One-dimensional (1-D) carbon nanostructures offer unique features for addressing these problems. The conductive matrix created by the one-dimensional carbon structural network provides better electrical connection to the active materials. In addition, novel designs of the 1-D carbon structures can potentially address the previously mentioned difficulties in engineering sulfur cathodes.

Hollow carbon nanofibers with a high aspect ratio have been shown to be effective in trapping sulfur (Fig. 4a).[17] The electrode was fabricated using a template synthesis method in which an anodized aluminum oxide (AAO) membrane was coated uniformly with a carbon thin film to form an array of hollow carbon nanofibers. Sulfur was then loaded into the hollow carbon nanofibers by mixing and heating to 155 °C. The presence of the AAO membrane prevents the coating of sulfur onto the outer walls of the carbon nanofibers, thus reducing the exposure of sulfur to the electrolyte (Fig. 4b). At the same time, the carbon walls provide conductive pathways for both electronic and ionic transport, allowing rapid reaction kinetics. The unique fabrication process enables trapping of sulfur–polysulfides within the hollow fibers and reduces deposition of sulfur on the external carbon surfaces, thus minimizing polysulfide dissolution. Electrochemical testing showed that this sulfur cathode delivered a high initial discharge capacity of around 1400 mAh g^{-1} with around 75% sulfur loading in the electrode and 1 mg cm^{-2} of sulfur content. The cycling capacity retention also showed significant improvement, with a reversible capacity of around 730 mAh g^{-1} after 150 cycles of charge–discharge (Fig. 4c).

Another approach that used similar 1-D hollow carbon structures involved high temperature treatment of a sulfur/hollow carbon tubes composite, which resulted in the intercalation of sulfur into the graphitic clusters and the amorphous carbon in the walls.[31] This approach allowed the sulfur electrode to achieve a stable specific capacity close to 700 mAh g^{-1} for about 80 cycles. The weight content of sulfur in this work is about 40%. The voltage profile in this report is slightly different
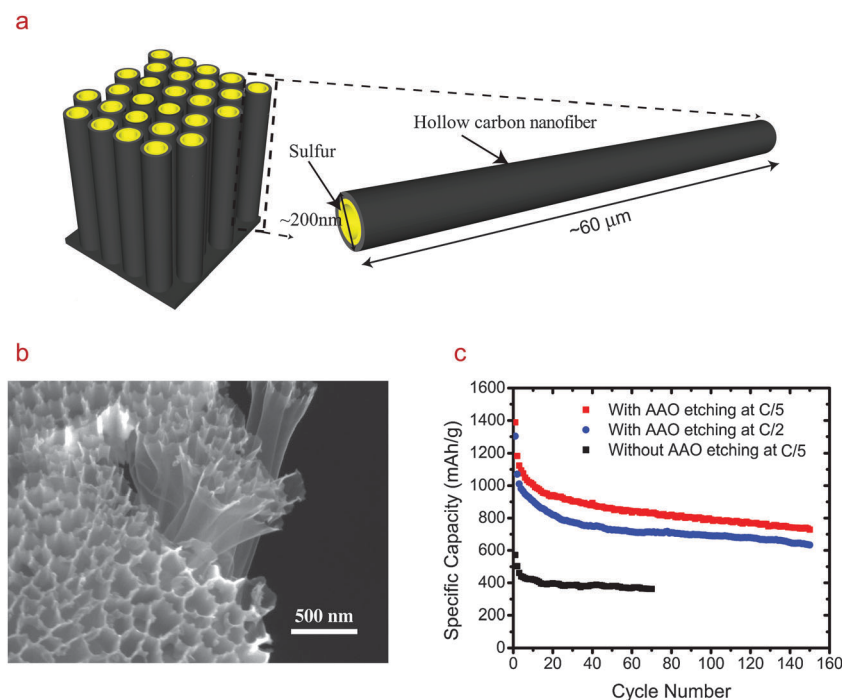

Fig. 4   Cathode made from sulfur encapsulated by hollow carbon nanofibers. (a) Schematic diagram of the high aspect ratio one-dimensional hollow carbon nanofiber–sulfur composite. (b) SEM image of the cathode after sulfur infusion and AAO etching. (c) Cycling performance of the sulfur cathode at $C/5$ and $C/2$. The black curve shows cycling performance of the sulfur cathode without AAO etching.[49] The figure is reprinted with permission from ref. 17.

from that of the conventional sulfur cathodes, in which a two-plateau behavior is observed for both the charge and discharge curves. The sloping galvanostatic charge–discharge profile is characteristic of a single-phase reaction and it suggests that the sulfur could have reacted with the carbon. The authors proposed that the originally orthorhombic S_8 might be converted to S_6 and S_2 with strong bonding to carbon defects in the graphite layers.

Other examples of using 1-D carbon nanostructures include various types of sulfur–carbon nanotube (CNT) composites, in which improved sulfur utilization and capacity retention have been generally reported.[50–52] Most of these works involved coating sulfur onto the CNT surface to obtain a core–shell structure. Although there is significant variation in the reported electrochemical performance, most sulfur–CNT electrodes can attain an initial specific capacity of around 1000 mAh g^{-1} with improved capacity retention as compared to simple mixing of sulfur particles and carbon.[53] Modification of the CNT surface has been shown to be beneficial in enhancing the capacity retention. Chen and co-workers demonstrated that when the CNTs were treated with nitric acid to incorporate carboxyl functional groups, the porous sulfur–CNT cathode delivered a relatively stable discharge capacity of about 800 mAh g^{-1}.[54] This demonstrates the importance of introducing hydrophilic groups to the conductive matrix in improving the cycling performance.

To reduce the amount of exposed sulfur in the electrode, porous carbon nanofibers have also recently been used for sulfur electrodes. In this approach, carbon nanofibers from commercial activated carbon cloth[55] or electrospun polymeric precursors[56] were impregnated with sulfur. The commercial activated carbon fibers have a narrower pore size distribution, with a majority of the microporous structures smaller than 2 nm. The small pore size allows more intimate contact between the sulfur and the conductive matrix. At the same time, the exposed sulfur area was reduced and dissolution of polysulfides into the electrolyte was attenuated. The activated carbon fiber cloth/sulfur composite delivered an initial discharge capacity of around 1000 mAh g^{-1} and the capacity decay was around 20% over 80 cycles. The discharge capacity of the activated carbon fiber–sulfur cathode increased slightly during the initial cycling, which was probably due to the gradual activation of sulfur in the micropores. One problem with this microporous carbon fiber structure is the relatively low sulfur to carbon ratio in the electrode. The use of carbon fiber cloth allows for the preparation of a freestanding, binder-free sulfur electrode. Nevertheless, the small pore size only accommodate around 33 wt% of sulfur in the electrode composite, despite a relatively high pore volume of around 1 cm^3 g^{-1}.

Despite the improvements in specific capacity and capacity retention with cycling, there is still some capacity decay with long term cycling in the above-mentioned electrode structures. It is inevitable that with these top-down approaches, where sulfur is impregnated into pre-synthesized carbon structures, there are still openings where polysulfides can escape the structure and dissolve into the electrolyte. Subsequent deposition of lithium sulfide and recharging to sulfur can cause significant changes in the electrode structure and result in capacity decay.

Further coating of the carbon structures, by using polymers or inorganic materials, can potentially enhance the capacity retention of the sulfur cathode.

2.4 Polymer–sulfur nanocomposites

Polymer–sulfur composites have been explored in addition to their carbon counterparts. Unlike carbon nanostructures, which usually require carbonization processes at high temperature (>600 °C) during fabrication, polymer-based processes are feasible below 100 °C since polymers are soluble or dispersible in various solvents. This advantage makes it possible to synthesize structures that are difficult to be realized as carbon–sulfur composites due to sulfur's low melting point of 113 °C, such as conformal coating layers to trap polysulfides. Moreover, the functional groups and unique chain structure of polymers indicate that inter and/or intra-chain bonding could further chemically confine sulfur and polysulfides.[57,58] Polymers are also generally mechanically soft and can even be self-healing,[59,60] which is beneficial for solving issues related to volume expansion and material pulverization. In addition, thanks to the development of electronically conductive polymers, conductivity is not an issue when employing polymers for sulfur cathodes.[61,62]

Recently, a three-dimensional, cross-linked, structurally stable sulfur–polyaniline (PANi) nanotube was reported with excellent cycling performance.[57] The polyaniline nanotube was formed first through a one-step self-assembly process in ice water. Next, sulfur and the polyaniline tubes were mixed together and heated to 280 °C so that sulfur is not only physically absorbed inside the tubes, but also reacts with the polymer to form inter- and/or intra-chain disulfide bonds (Fig. 5a). This well-designed structure retained a capacity of 568 mAh g^{-1} after 100 cycles and 432 mAh g^{-1} after 500 cycles at a rate of 1 C, which corresponds to a capacity retention of 76% after 400 cycles (Fig. 5b). Higher capacity (over 900 mAh g^{-1}) and good capacity retention were also achieved at a lower rate of 0.1 C. The authors attribute the capacity decay to two factors: (1) there might still be some dissolution and shuttling of the polysulfide species, and (2) the S/PANi polymer framework formed *in situ* is electrochemically active, so the disulfide bonds split and recombine during discharge–charge. It is possible that some of the dissociated disulfide bonds cannot recover to the original cross-linked state, causing a decrease in the stability of the polymer matrix. The content of sulfur in the PANi/sulfur composite is determined to be 62% by Thermogravimetric Analysis (TGA) and the electrode contains 80% PANI/sulfur composite.

PAN/sulfur composites have also been reported with excellent cycle life.[63–66] For fabrication of such composites, sulfur and PAN were heated together between 250 and 600 °C. Sulfur reacted with PAN at these high temperatures to form a heterocyclic polymer interconnected with disulfide bonds on the side chain. Unreacted sulfur also formed small nanoparticles (<10 nm) that were well embedded in the polymer matrix.[63,64] Such chemically bonded sulfur showed a good cycling retention of 90% up to 380 cycles,[66] but the operating voltage was less than 2.0 V and the sulfur content was not high. Nevertheless, this demonstrates that organic disulfide bonding to polymer chains can result in good
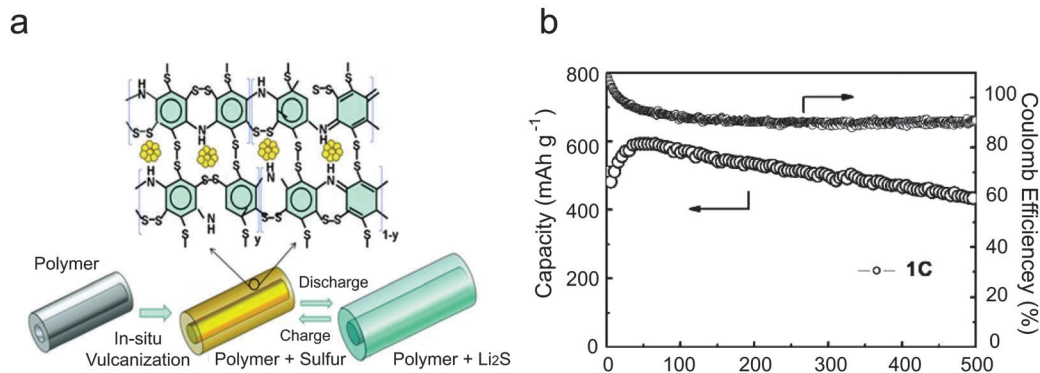
3024 | *Chem. Soc. Rev.*, 2013, **42**, 3018–3032

This journal is © The Royal Society of Chemistry 2013

a

b

Fig. 5 (a) Schematic illustration of the construction and discharge–charge process of the PANi nanotube/sulfur composite. (b) Prolonged cycling performance and Coulombic efficiency of the electrode up to 500 cycles at a 1 C rate.[57] The figure is reprinted with permission from ref. 57.

electrochemical reversibility, showing that this approach is promising for high performance Li/S batteries.

Hybrid carbon–polymer structures have also been explored to improve the performance of the sulfur cathode.[26,27] Though nanoporous carbon structures are effective for trapping polysulfides, polysulfides can still diffuse out of the structure over a prolonged time if there is no effective capping layer surrounding the carbon/sulfur particles. For example, CMK-3 mesoporous carbon particles have a diameter of 0.5–1 μm and thus the surface area exposed to the electrolyte is considerable. Additional polymer coating can help further trap polysulfides. Poly(3,4-ethylenedioxythiophene)-based polymers have been demonstrated to enhance the electrochemical performance of porous carbon–sulfur composites.[26,27] For instance, after coating with poly(3,4-ethylenedioxythiophene)–poly(styrene sulfonate) (PEDOT:PSS), the Coulombic efficiency of the CMK-3/sulfur electrode was improved from 93% to 97%, and the capacity decay was reduced from 40% per 100 cycles to 15% per 100 cycles during long term cycling.[26] The content of sulfur is $\sim$43% in the electrode with a total mass loading of 1 mg cm^{-2}. However, fast initial decay is still observed in the polymer-coated samples. Further optimization and understanding of the mechanism is needed to achieve more stable cycling performance.

In general, the chain-like structure and rich functional groups of polymers facilitate chemical trapping of polysulfides while maintaining good physical confinement in a similar manner as carbon. In addition, the mechanical properties of polymers allows for better accommodation of volume expansion than pure carbon coatings. These merits offer exciting opportunities for designing sulfur cathodes with superior performance. However, the long term stability and swelling of polymers in organic electrolytes need to be further investigated.

2.5 Nanostructured additives and binders

The use of adsorbing material to trap lithium polysulfides has been proposed in a number of publications. Such additives include carbon, silica, aluminum oxide, transition metal chalcogenides and metals.[67–70] Although the exact mechanisms of the metal oxide–polysulfide interaction are still unclear, it is generally observed that the addition of such particles can improve the cycling performance and Coulombic efficiency.

One notable development in this area is the work by Ji et al., where SBA-15 mesoporous silica was used as a reservoir for trapping polysulfides.[70] The mesoporous silica is inert to the redox reaction, so the pores are less likely to be blocked by the reduced lithium sulfide deposits. It was demonstrated that the highly porous silica could reversibly adsorb and desorb the polysulfides during the charge–discharge process (Fig. 6a–c). Both the initial discharge capacity and Coulombic efficiency were significantly improved with the addition of SBA-15 (Fig. 6d). With the mesoporous silica additives, the authors were able to achieve a reversible capacity of around 650 mAh g^{-1} after 40 cycles at C/5 (Fig. 6e). The mass loading of sulfur is 1.2 mg cm^{-2}, which is 60% of the total weight on the electrode.

Metal–organic-framework (MOF) has also been recently studied by Demir-Cakan et al. as an additive for sulfur cathodes.[53] The MOF that was utilized, MIL-100, has a small aperture window of around 5–8.6 Å, which can potentially slow down the diffusion of polysulfides. It was proposed that the surface activity of the mesoporous additives, in addition to the pore sizes, plays a very important role in enhancing the cathode performance. This was revealed by the X-ray photoelectron spectroscopy (XPS) spectrum, in which the S 2p peak shifted to a lower binding energy after impregnation of sulfur in MOF. The authors also took a further step to compare the performance of sulfur cathodes with SBA-15, MOF and mesoporous carbon additives. The better capacity retention in cells with SBA-15 and MOF was explained in terms of the stronger interaction between the charged species and the more polarized oxygenated surfaces. Overall, the improvement in sulfur cathode performance due to the presence of these additives is highly promising. Further research is required to decipher the trapping mechanism of polysulfides in these mesoporous oxygenated architectures. Due to the difficulty in the experimental characterization of the highly air- and water-sensitive polysulfide species, first-principles calculations could offer an alternative for understanding the atomic-level interactions.

One problem with such nanostructured additives is the extra cost and weight involved. Most of the materials utilized require
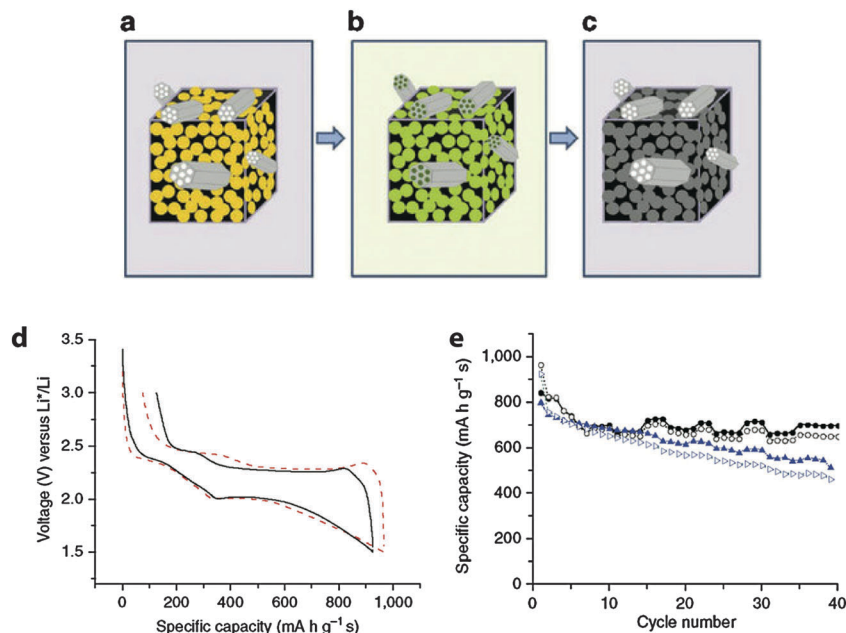
Fig. 6 ''Polysulfide reservoir'' concept afforded by the SBA-15 platelets in the SCM/S electrode. (a) Sulfur electrode embedded with SBA-15 before discharge. (b) Absorption of polysulfides by SBA-15 during discharge. (c) Release of polysulfides by SBA-15 at the end of discharge. (d) Comparison of the discharge profile of the first cycle of SCM/S (black solid line) and SCM/S with the SBA-15 additive (red dotted line). (e) Comparison of the cycling stability of SCM/S (blue) and SCM/S with SBA-15 additive (black) showing the capacity stabilization effect of SBA-15.[70] The figure is reprinted with permission from ref. 70.

elaborate fabrication processes that could potentially undermine the economic viability of lithium sulfur batteries. To combat this problem, polymer additives, which are also used as binders in the sulfur electrode, can also be engineered to provide better trapping of polysulfides.

Several alternative electrode binders have been studied to replace the commonly used polyvinylidene difluoride (PVDF) binder. The idea is to incorporate functionalities on the polymer binders so as to improve their interaction with the polysulfide species. In addition, some of the aqueous binders (*e.g.* styrene butadiene rubber and sodium carboxylmethyl cellulose) that have been studied allow for better dispersion of the electrode materials and greater structural stability.[71] Gelatin is another interesting water-soluble macromolecule that has been shown to significantly improve the cycling performance of the sulfur cathode. As an ampholytic molecule comprised of amino acid subunits, gelatin displays hydrophilic properties and can enhance the dispersion of sulfur particles in the composite cathode framework.[72] X-ray diffraction (XRD) and differential scanning calorimetry (DSC) results have demonstrated that the presence of gelatin could significantly improve the redox reversibility of the lithium–sulfur reaction, with the S_8 signal being detected at the end of the charge cycle.[73] The sulfur cathode with a gelatin binder was shown to deliver a discharge capacity of around 700 mAh g^{-1} for 50 cycles. In addition, the generation of pores inside the gelatin–sulfur composite cathode has also been shown to improve the rate capability of the electrode, with a reversible capacity of around 500 mAh g^{-1} achieved at a 1 C rate.[74]

Other binders that have been studied include polytetrafluoroethylene (PTFE) + carboxymethylcellulose (CMC),[75] Nafion,[76] and polyvinylpyrrolidone (PVP)–polyethyleneimine (PEI).[77] These aqueous binders provide a strong adhesion for the sulfur cathode.

Although many of the alternative binders have shown some sort of advantages over PVDF in one way or another, there has not yet been significant adoption of these new materials. PVDF by and large is still the most commonly used binder for the sulfur cathode. This is probably due to a lack of understanding of how these binders interact with the sulfur cathode to improve performance. With its good adhesion and stability in the electrochemical environment, PVDF is still the best compromise among all the binders at the moment.

2.6 Nanostructured Li_2S electrodes

Besides the sulfur cathode, the lithium anode also presents significant challenges.[15,16] First, there are safety concerns due to its high reactivity and the tendency to form dendrites during Li plating, especially for applications in electric vehicles. Second, the lithium anode usually exhibits a lower Coulombic efficiency ($<99\%$) than anode materials in Li-ion batteries.[15,78] It is important to note that in commercial batteries, the amount of lithium in the anode would be limited and balanced with the amount of sulfur in the cathode, while in lab-scale half-cells, lithium always presents in significant excess. The low Coulombic efficiency of lithium metal dissolution and re-deposition and lithium's high reactivity towards the electrolyte indicate that extra electrolyte and lithium are needed to compensate for the loss of material due to side reactions. The excess lithium and electrolyte required could significantly lower both the volumetric and gravimetric energy density of the Li/S battery. This serious challenge should be explored in future studies.

3026 | *Chem. Soc. Rev.*, 2013, **42**, 3018–3032

This journal is © The Royal Society of Chemistry 2013

One approach to solve this problem is to start with Li_2S instead of sulfur in the cathode. Since lithium is stored in the Li_2S positive electrode, the metallic lithium anode can be replaced by a high-capacity tin or silicon anode. Moreover, Coulombic efficiency as high as 99.94% has been reported in the silicon anode.[79] Li_2S has a high specific capacity of 1166 mAh g^{-1} and a voltage profile that is similar to the sulfur cathode. The main hindrance to utilizing Li_2S is that it is both electronically and ionically insulating.[80] Our measurements show that stoichiometric Li_2S has an electronic resistivity higher than 10^{14} ohm cm, and the Li^+ diffusivity in Li_2S is as low as 10^{-15} cm^2 s^{-1}.[12] As a result of these low values, Li_2S has traditionally been considered electrochemically inactive.[81] Discharge capacities around 300 mAh g^{-1} were also observed in micron-sized carbon–Li_2S composite particle electrodes at room temperature.[82,83] Nagao *et al.* combined micron-sized Li_2S particles with a solid electrolyte, and a capacity of 700 mAh g^{-1} was achieved at the low current rate of 0.03 C.[84]

Given the fact that Li_2S has both low electronic conductivity and poor ionic diffusivity, nanostructuring Li_2S is a feasible and practical approach to improve its rate capability and decrease the voltage hysteresis. Guided by this idea, we synthesized a mesoporous carbon–Li_2S nanocomposite by chemically lithiating a CMK-3 carbon–sulfur composite with *n*-butyllithium.[80] It is supposed that this strong reductant reduced sulfur to Li_2S through the reaction

$$2C_4H_9\text{–}Li + 2S \rightarrow C_4H_9\text{–}S\text{–}C_4H_9 + 2Li_2S$$

The thioether byproduct was evaporated afterwards by heating. This lithiation process resulted in Li_2S that was trapped in the several nanometer-diameter pores of the CMK-3, and thus fast kinetics could be achieved (Fig. 7a and b).[80] It was found that only 60% of the original sulfur remained in the electrode, as measured by atomic emission spectroscopy (AES), which was much less than the value used in our original report.[80] An initial discharge capacity of 950 mAh g^{-1} was achieved based on the mass of Li_2S, which is ~80% of the theoretical value and thirty times that of 10 μm-sized commercial Li_2S particles (Fig. 7c). The specific capacity in this work is based on the mass of Li_2S instead of sulfur. After some initial decay, the capacity becomes stabilized at 600 mAh g^{-1}. The voltage hysteresis of the cathode is as small as 0.2 V due to the small dimensions of Li_2S. Full cells based on a carbon–Li_2S composite cathode and a silicon nanowire anode showed an initial discharge capacity of 803 mAh g^{-1} at $C/8$ (146 mA g^{-1}), and it remained at 656 mAh g^{-1} at a 1 C rate. Importantly, the voltage hysteresis is only 0.4 V at $C/8$ for the full cell, leading to energy efficiency as high as 80%. The percentage of Li_2S in the electrode is 37% and the mass loading is around 0.7–0.8 mg Li_2S per cm^2.

Besides the CMK-3/Li_2S nanocomposite, micron-sized Li_2S electrodes have also been made by ball milling.[84,85] The ball-milled electrode shows a high specific capacity close to the theoretical value of Li_2S, but large voltage hysteresis, as illustrated in Fig. 7d.[85] In addition, recently a universal over-charging method has been proposed to activate Li_2S particles from nano-size to ~10 μm.[12]

Along with pure Li_2S electrodes, Li_2S–metal hybrid cathodes have also been studied, including the Li_2S–Fe system in liquid
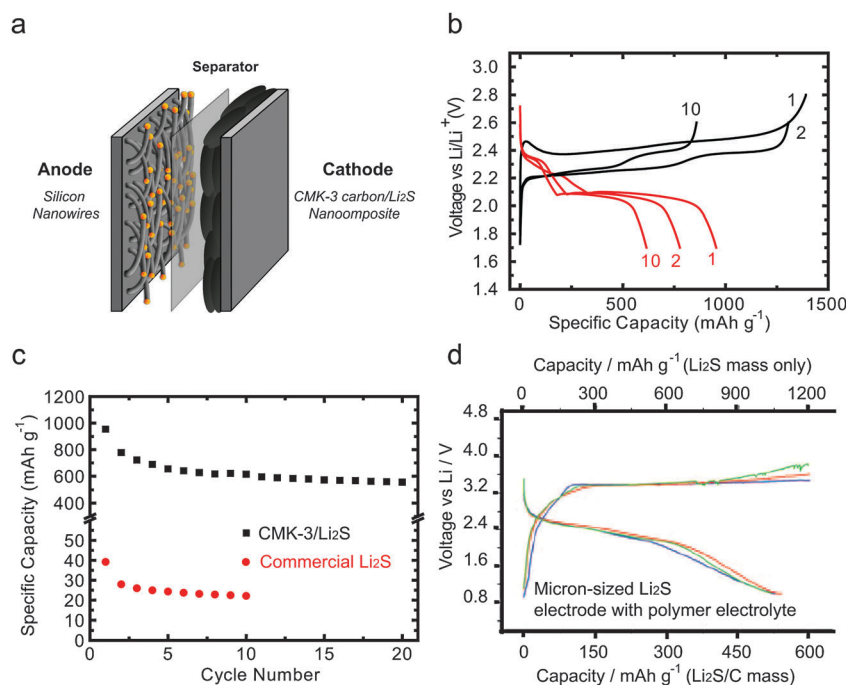

Fig. 7 (a) A schematic of a CMK-3 mesoporous carbon-embedded Li_2S/silicon nanowire battery. (b) The voltage profile of a CMK-3/Li_2S cathode *versus* a lithium anode. (c) The cycling performance of a CMK-3/Li_2S cathode compared to a commercial 10 μm-sized Li_2S particle electrode. (d) Typical capacity delivery in multiple charge–discharge cycles (1 blue, 2 red, 3 green) of a Li_2S/C electrode in a polymer electrolyte. Lithium metal counter and reference electrode. The operating temperature is 60 °C and the cycling rate is $C/20$ (C = 2.2 mA cm^{-2}). The upper and bottom axes represent capacity based on the mass of Li_2S and Li_2S–carbon, respectively. The figures are reprinted with permission from ref. 80 and 82.

This journal is © The Royal Society of Chemistry 2013

Chem. Soc. Rev., 2013, 42, 3018–3032 | 3027

electrolyte[81] and Li$_2$S–Co[86] and Li$_2$S–Cu[87] electrodes with solid electrolytes. In these systems, the chemistry is altered to M + xLi$_2$S → MS$_x$ + 2xLi$^+$ + 2xe$^-$, but not Li$_2$S → S + 2Li$^+$ + 2e$^-$. Consequently, the voltage is lowered to between 1 and 2 V and the specific capacity is lower since transition metals are much heavier than carbon.

Developments in Li$_2$S-based electrodes have revealed alternative ways to achieve high energy density. Further studies to optimize the synthesis of Li$_2$S nanostructures and to understand the nature of the electrochemical reactions are needed to improve the performance of this material. It should also be noted that Li$_2$S can react with moisture to generate toxic H$_2$S so that a dry room or glovebox is necessary for electrode fabrication and assembly.

2.7 Novel electrolytes and electrolyte additives

Another component in the lithium sulfur system that has attracted significant attention is the electrolyte. Although this part of battery is not necessarily related to nanostructured materials, its importance in developing viable lithium sulfur batteries warrants some discussion here.

Many types of electrolytes, including ether, sulfone, carbonates, and ionic liquid, have been investigated for their effect on the performance of sulfur cathodes. Electrolytes could have a significant effect on the lithium sulfur batteries performance due to the variation in solubility of and chemical interaction with polysulfides. Carbonate based electrolytes generally do not work well in lithium sulfur batteries due to the nucleophilic attack of the carbonyl group by the polysulfide anion.[88] Ether solvents such as 1,3-dioxolane (DOL), 1,2-dimethoxyethane (DME),[89] and tetra(ethylene glycol) dimethyl ether (TEGDME)[90] are preferred due to the high solubility of polysulfides, good ionic conductivity and low viscosity. Alky sulfone electrolytes such as ethyl methyl sulfone (EMS) are also sometimes used. Sulfone based electrolytes are considered to be highly stable with respect to oxidation at the cathode, but its effect specific to sulfur electrode was not very well studied. Ionic liquid based electrolytes were studied by Shin and Cairns.[91] Ionic liquid is normally mixed with ether solvent (*e.g.* PEGDME) in order to reduce its viscosity and improve the ionic conductivity.

One of the most important electrolyte additives used in lithium sulfur batteries is lithium nitrate (LiNO$_3$), which has been extensively studied for its effect on cell performance.[78,92] Although the detailed chemical reactions of LiNO$_3$ inside the battery are not fully understood, it has been suggested that the oxidizing additive forms a stable passivation layer (Li$_x$NO$_y$ and Li$_x$SO$_y$) on the lithium metal surface.[92] This passivation layer can effectively slow down the reduction of polysulfide species at the lithium surface and result in higher Coulombic efficiency close to 98–99%. The passivating effect of LiNO$_3$ at the lithium metal surface has also allowed researchers to use liquid lithium polysulfides as a catholyte.[93,94] Such batteries use higher order lithium polysulfide (*e.g.* Li$_2$S$_9$) as a catholyte and porous carbon as a current collector. A specific capacity of around 600 mAh g^{-1} has been obtained for over 60 cycles. Despite the promising performance, however, the capacity decay issue still

exists in these types of battery systems. This implies that the shuttle effect is no longer a major issue in Li/S batteries if LiNO$_3$ is present in the electrolyte.

Another interesting development in the area of electrolyte is the use of ionic liquid. The adoption of ionic liquid electrolytes has not been widespread, mainly due to their high viscosity, low electrode wettability and high cost. Nevertheless, mixtures of ionic liquid with ether-based solvents (such as PEGDME) have been shown to improve the thermal stability and ionic conductivity of the electrolyte.[95] Recent reports of graphene oxide/sulfur composite cathodes also demonstrated improved cycling performance in ternary electrolytes containing ionic liquid.[45]

3. Characterization of nanostructured sulfur cathodes

The chemistry of sulfur cathode is very complicated, as multiple steps are involved during discharge and charge. In discharge, sulfur is reduced to soluble lithium polysulfides first which then redeposits onto the cathode as solid Li$_2$S$_2$ and Li$_2$S. It is critical to understand the detailed mechanisms involved in this process to guide researchers towards designing better sulfur electrodes. Unfortunately, it is difficult to obtain information on the morphological, structural and compositional evolution of the sulfur cathode due to the following reasons: (1) sulfur has a low melting point and a high vapor pressure at room temperature so that it is only stable for a short time in high vacuum, (2) polysulfides and Li$_2$S are not air-stable; they react quickly with moisture and oxygen, (3) polysulfides are soluble in the electrolyte and thus it is difficult to use conventional means to understand phase transformations during the intermediate stages of charge and discharge, and (4) the sulfur cathode is not necessarily stable when electrically disconnected: the rest time between the end of electrochemical operation and characterization may result in changed properties. Due to these limitations, there are many controversies related to the details of the Li/S battery chemistry; however, thanks to tremendous efforts in this area, more and more knowledge has been accumulated and we now have a clearer picture of the true chemistry of the battery. Sulfur cathodes have been characterized by various techniques, such as SEM,[96–98] TEM,[13,99] AFM,[13] Raman,[13,49,100] XRD,[97,98,101–104] X-ray Absorption Spectroscopy (XAS)[88] and X-ray imaging.[105] In this part, we will review reports on *ex situ* experiments first and then move to *in situ* characterization, which gives more unambiguous information.

Ex situ SEM studies typically show that most sulfur in the cathode disappears at the end of the high plateau as polysulfides diffuse into the electrolyte. The electrode is covered by a film at the end of discharge due to the precipitation of Li$_2$S$_2$ and Li$_2$S.[96,97] The *ex situ* XRD results are more controversial. Many reports show the formation of crystalline Li$_2$S by the end of the discharge and no oxidation to crystalline sulfur by the end of the charge cycle.[96,98,102–104] Two outliers to these results are the work done by Wang *et al.* using gelatin as a binder, where elemental sulfur diffraction peaks reappeared after a full

3028 | *Chem. Soc. Rev.*, 2013, **42**, 3018–3032

This journal is © The Royal Society of Chemistry 2013

charge, even after 50 cycles,[101] and the work by Elazari *et al.* studying Li/S batteries from Sion Power Inc., which used electron diffraction to show that crystalline sulfur remained after full discharge in cells cycled fewer than 10 times; Li_2S was only evident in discharged cells cycled more than 10 times.[13] These controversies will further be discussed in relation to *in situ* experiments in the following paragraphs. AFM has also been used to understand the morphological evolution of the sulfur cathode during cycling.[13] It is observed that the electrode morphology changes from cycle to cycle. Moreover, the fraction of conductive surface area on the electrode decreases down to nearly zero after only 30 cycles. Though the authors consider that the bulk of the electrode remains in a continuous conductive network, these changes in morphology and properties may play an important role in the capacity fade.

Ex situ studies have significantly broadened the community's understanding of sulfur cathodes. However, the post-treatment and inevitable exposure to air may lead to spurious observation and misguided interpretation of the mechanism involved. For example, washing away the electrolyte to obtain a clean sample for XRD and microscopic characterization could remove sulfur at the same time, which may contribute to the differing observations of whether elemental sulfur reappears or not at the end of charging. As a result, *in situ* techniques are crucial to obtain unambiguous information.

There have been a limited number of studies on *in situ* probing of sulfur cathodes. Recently, progress has been made towards *in situ* and *in-operando* X-ray characterization of sulfur cathodes, and the results are quite different from *ex situ* studies.[105] It was found that crystalline Li_2S does not form at the end of discharge, but that the discharge product transforms to crystalline Li_2S after resting in a disconnected state for seven days. Moreover, whether crystalline sulfur reappears at the end of charging was found to depend on the morphology of the electrode framework. No diffraction peaks of sulfur were found after charging of graphene-wrapped sulfur and micron-sized sulfur particles. In contrast, crystalline sulfur was observed in a Super P carbon–sulfur composite. The mechanism behind these observations is still unclear, but it may depend on how the sample is prepared. The effect of resting the cell on the phase evolution of sulfur and Li_2S illustrates the importance of *in situ* studies.

In situ X-ray imaging also shows different results from previous *ex situ* observations. The X-ray image reflects the spatial distribution of the intensity of the transmitted beam with a resolution of ~30 nm.[106,107] Since the absorption of X-rays is sensitive to the atomic number of the element considered, good contrast is obtained between sulfur and the surrounding electrode structure. When using X-ray imaging on sulfur particles during *in situ* discharging, a slight decrease in size was noted in the first half of the high plateau and the particle looked more porous, while images of particles remained intact during the following cycles.[105] Quantitative calculations of the contrast between the sulfur particle and the background also show the same trend: the sulfur content in the particle decreases slightly in the high plateau during initial
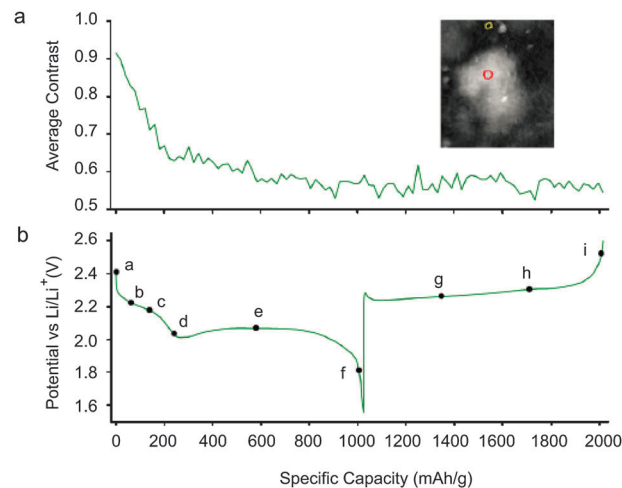

Fig. 8 (a) Changes in average contrast *vs.* specific capacity in Transmission X-ray Microscopy (TXM) micrographs of a Li/S battery cycled at C/8 and (b) the cell potential. The inset of (a) is the X-ray image of a sulfur particle. The red and yellow circles represent the sample and background area, respectively, for calculating the contrast.[105] The figure is reprinted with permission from ref. 105.

discharge, but it remains constant in the following low plateau and charging step (Fig. 8). This suggests that although some polysulfides diffuse into the electrolyte, the majority of the active material is not lost. This is distinct from *ex situ* SEM observations, where polysulfides do not remain in the electrode at the end of the high plateau since they are washed away in the post-treatment. Considering that the cycle life of these cells remains poor, this suggests that other factors such as volume expansion and the insulating nature of Li_2S are major reasons for the poor cycle life. In addition, *in situ* XAS has been reported recently to understand the effect of the electrolyte on the electrochemical behavior of the sulfur cathode.[88] Overall, these results highlight the importance of *in situ* characterization of Li/S batteries to eliminate artifacts introduced in post-treatment for *ex situ* studies.

Further *in situ* characterization of sulfur cathodes with diverse techniques is desired to fully understand the charge–discharge mechanisms. For example, *in situ* AFM studies could provide information on the local volume changes during charge and discharge. *In situ* TEM characterization would lead to a deeper and more accurate understanding of the compositional and structural evolution.

4. Conclusion and outlook

In the past few years, various nanostructures have been realized to improve the performance of sulfur cathodes, such as different carbon–sulfur nanocomposites, polymer–sulfur nanocomposites and nanostructured Li_2S electrodes. These rational and creative designs help solve the interrelated challenges of volume expansion, poor ionic and electronic transport and polysulfide dissolution in the Li/S battery, and thus dramatically enhance the capacity, cycle life and power capability of sulfur cathodes. These developments represent promising

Table 2 Estimation on the volumetric energy density of the Li/S battery and the LiMO$_2$/graphite battery (electrode materials are considered)

	Specific capacity of cathode (mAh g^{-1})	Tap density (g cm^{-3})	Content of active materials	Full cell voltage (V)	Volumetric energy density of full cell (Wh L^{-1})
Current Li/S battery	900	1	60%	2.15	770[a]
Projected Li/S battery	1200	1	75%	2.15	1050[a]
LiMO$_2$/graphite[b]	160	3	90%	3.65	760[c]

[a] The capacity of lithium is supposed to be 2000 mAh g^{-1} to include the extra lithium needed for long term cycling. [b] M = Ni$_{1/3}$Mn$_{1/3}$Co$_{1/3}$. [c] The parameters for the graphite anode are 350 mAh g^{-1}, 1.2 g cm^{-3} and 95% content.

steps towards a viable Li/S battery. Moreover, a deeper and broader understanding of the lithium–sulfur reaction mechanism has also been obtained based on *in situ* and *ex situ* nano-characterization techniques. However, there are still many issues to explore in this electrochemical system. First, a comprehensive understanding of the chemistry is needed. Since it is more difficult to characterize the sulfur cathode than other battery materials, many details of the electrochemical mechanisms involved are controversial and unclear. Further studies, especially *in situ* approaches, would help build a thorough understanding of the reaction mechanisms and would lead to an optimized design for the electrode.

Besides further improving the cycle life of the Li/S battery, another topic to explore is improving the content of sulfur and the tap density of the whole electrode, which are crucial to the volumetric energy density of real products. Li/S battery has a much higher gravimetric energy density than state-of-the-art Li-ion batteries, but it may not outperform Li-ion batteries when volumetric energy density is considered. Sulfur has a low density (2.07 g cm^{-3}) compared to transition metal oxides (4–5 g cm^{-3}) and phosphates (3.6 g cm^{-3}), which decreases its volumetric energy density. The volumetric energy density is further lowered since more conductive carbon additive is needed for the operation of sulfur cathodes. The typical sulfur content is 40–65 wt% in the majority of academic reports, while traditional battery materials require less than 20 wt% additives. In addition, nanostructures also lead to lower tap densities than micron-sized particles. Table 2 presents the volumetric energy density of the state-of-the-art LiMO$_2$–graphite battery and the current and projected Li/S battery system. Only parameters of active materials and electrode additives (*e.g.* carbon black and binder) are considered here. The current Li/S battery could have an energy density slightly higher than the LiMO$_2$–graphite system, and future improvement may lead to an energy density around 1000 Wh L^{-1}, which is ~40% higher than state-of-the-art LiMO$_2$–graphite batteries. Novel approaches, which utilize close to the theoretical capacity (>1500 mAh g^{-1}) while maintaining high sulfur content (>75%), are needed to realize a Li/S battery with volumetric energy density well beyond the limit of Li-ion batteries.

Finally, in addition to the issue of volumetric energy density, there are few reports on important characteristics like self-discharge and high/low temperature performance.[108,109] Since polysulfides are soluble in the electrolyte, more issues may arise than in other battery chemistries related to self-discharge and degradation at high temperature. The insulating nature of

the active materials could also lead to concerns for power capability at low temperature. These issues need to be evaluated carefully as they are important for the commercialization of Li/S batteries.

Though there are still many challenges on the road to a viable Li–S battery, the progress achieved in the past five to ten years has been significant. Major advances have been made in both enhancing the performance and understanding the mechanisms of Li–S batteries. We believe that further studies by the battery community will lead to more exciting results and eventually practical Li–S cells.

Acknowledgements

References

1 J. M. Tarascon and M. Armand, *Nature*, 2001, **414**, 359–367.
2 M. Armand and J.-M. Tarascon, *Nature*, 2008, **451**, 652–657.
3 M. S. Whittingham, *Chem. Rev.*, 2004, **104**, 4271–4301.
4 X. L. Ji and L. F. Nazar, *J. Mater. Chem.*, 2010, **20**, 9821–9826.
5 M. Z. Jacobson, *Energy Environ. Sci.*, 2009, **2**, 148–173.
6 P. G. Bruce, S. A. Freunberger, L. J. Hardwick and J.-M. Tarascon, *Nat. Mater.*, 2012, **11**, 19–30.
7 D. Herbert and J. Ulam, *U.S. Patent*, 3043896, 1962.
8 J. R. Birk and R. K. Steunenberg, *Adv. Chem. Ser.*, 1975, 186–202.
9 Y. V. Mikhaylik and J. R. Akridge, *J. Electrochem. Soc.*, 2004, **151**, A1969–A1976.

10 K. Kumaresan, Y. Mikhaylik and R. E. White, *J. Electrochem. Soc.*, 2008, **155**, A576–A582.

11 H. Yamin and E. Peled, *J. Power Sources*, 1983, **9**, 281–287.

12 Y. Yang, G. Y. Zheng, S. Misra, J. Nelson, M. F. Toney and Y. Gui, *J. Am. Chem. Soc.*, 2012, **134**, 15387–15394.

13 R. Elazari, G. Salitra, Y. Talyosef, J. Grinblat, C. Scordilis-Kelley, A. Xiao, J. Affinito and D. Aurbach, *J. Electrochem. Soc.*, 2010, **157**, A1131–A1138.

14 S. Joongpyo, K. A. Striebel and E. J. Cairns, *J. Electrochem. Soc.*, 2002, **149**, A1321–A1325.

15 C. Brissot, M. Rosso, J. N. Chazalviel and S. Lascaud, *J. Power Sources*, 1999, **81**, 925–929.

16 X. H. Liu, L. Zhong, L. Q. Zhang, A. Kushima, S. X. Mao, J. Li, Z. Z. Ye, J. P. Sullivan and J. Y. Huang, *Appl. Phys. Lett.*, 2011, **98**, 183107.

17 G. Zheng, Y. Yang, J. J. Cha, S. S. Hong and Y. Cui, *Nano Lett.*, 2011, **11**, 4462–4467.

18 J. L. Wang, J. Yang, J. Y. Xie, N. X. Xu and Y. Li, *Electrochem. Commun.*, 2002, **4**, 499–502.

19 J. Wang, *Electrochim. Acta*, 2003, **48**, 1861–1867.

20 C. D. Liang, N. J. Dudney and J. Y. Howe, *Chem. Mater.*, 2009, **21**, 4724–4730.

21 X. L. Ji, K. T. Lee and L. F. Nazar, *Nat. Mater.*, 2009, **8**, 500–506.

22 S. Jun, S. H. Joo, R. Ryoo, M. Kruk, M. Jaroniec, Z. Liu, T. Ohsuna and O. Terasaki, *J. Am. Chem. Soc.*, 2000, **122**, 10712–10713.

23 G. L. Miessler and D. A. Tarr, *Inorganic Chemistry*, Pearson Education, 1998.

24 G. He, X. L. Ji and L. Nazar, *Energy Environ. Sci.*, 2011, **4**, 2878–2883.

25 B. Zhang, X. Qin, G. R. Li and X. P. Gao, *Energy Environ. Sci.*, 2010, **3**, 1531–1537.

26 Y. Yang, G. H. Yu, J. J. Cha, H. Wu, M. Vosgueritchian, Y. Yao, Z. N. Bao and Y. Cui, *ACS Nano*, 2011, **5**, 9187–9193.

27 X. Li, Y. Cao, W. Qi, L. V. Saraf, J. Xiao, Z. Nie, J. Mietek, J.-G. Zhang, B. Schwenzer and J. Liu, *J. Mater. Chem.*, 2011, **21**, 16603–16610.

28 N. Jayaprakash, J. Shen, S. S. Moganty, A. Corona and L. A. Archer, *Angew. Chem., Int. Ed.*, 2011, **50**, 5904–5908.

29 J. Schuster, G. He, B. Mandlmeier, T. Yim, K. T. Lee, T. Bein and L. F. Nazar, *Angew. Chem., Int. Ed.*, 2012, **51**, 3591–3595.

30 S.-R. Chen, Y.-P. Zhai, G.-L. Xu, Y.-X. Jiang, D.-Y. Zhao, J.-T. Li, L. Huang and S.-G. Sun, *Electrochim. Acta*, 2011, **56**, 1–7.

31 J. Guo, Y. Xu and C. Wang, *Nano Lett.*, 2011, **11**, 4288–4294.

32 A. K. Geim and K. S. Novoselov, *Nat. Mater.*, 2007, **6**, 183–191.

33 H. Wang, J. T. Robinson, G. Diankov and H. Dai, *J. Am. Chem. Soc.*, 2010, **132**, 3270–3271.

34 H. Wang, H. S. Casalongue, Y. Liang and H. Dai, *J. Am. Chem. Soc.*, 2010, **132**, 7472–7477.

35 H. L. Wang, L.-F. F. Cui, Y. A. Yang, H. Sanchez Casalongue, J. T. Robinson, Y. Y. Liang, Y. Cui, H. J. Dai and H. S. Casalongue, *J. Am. Chem. Soc.*, 2010, **132**, 13978–13980.

36 H. Kim, S.-W. Kim, Y.-U. Park, H. Gwon, D.-H. Seo, Y. Kim and K. Kang, *Nano Res.*, 2010, **3**, 813–821.

37 S. Yang, G. Cui, S. Pang, Q. Cao, U. Kolb, X. Feng, J. Maier and K. Müllen, *ChemSusChem*, 2010, **3**, 236–239.

38 D. Wang, D. Choi, J. Li, Z. Yang, Z. Nie, R. Kou, D. Hu, C. Wang, L. V. Saraf, J. Zhang, I. A. Aksay and J. Liu, *ACS Nano*, 2009, **3**, 907–914.

39 H. L. Wang, Y. Yang, Y. Y. Liang, L. F. Cui, H. S. Casalongue, Y. G. Li, G. S. Hong, H. J. Dai and Y. Cui, *Angew. Chem., Int. Ed.*, 2011, **50**, 7364–7368.

40 H. Wang, Y. Yang, Y. Liang, J. T. Robinson, Y. Li, A. Jackson, Y. Cui and H. Dai, *Nano Lett.*, 2011, **11**, 2644–2647.

41 D. R. Dreyer, S. Park, C. W. Bielawski and R. S. Ruoff, *Chem. Soc. Rev.*, 2010, **39**, 228–240.

42 S. Park and R. S. Ruoff, *Nat. Nanotechnol.*, 2009, **4**, 217–224.

43 J.-Z. Wang, L. Lu, M. Choucair, J. A. Stride, X. Xu and H.-K. Liu, *J. Power Sources*, 2011, **196**, 7030–7034.

44 J. Liu, Y. L. Cao, X. L. Li, I. A. Aksay, J. Lemmon, Z. M. Nie and Z. G. Yang, *Phys. Chem. Chem. Phys.*, 2011, **13**, 7660–7665.

45 L. Ji, M. Rao, H. Zheng, L. Zhang, Y. Li, W. Duan, J. Guo, E. J. Cairns and Y. Zhang, *J. Am. Chem. Soc.*, 2011, **133**, 18522–18525.

46 N. Li, M. Zheng, H. Lu, Z. Hu, C. Shen, X. Chang, G. Ji, J. Cao and Y. Shi, *Chem. Commun.*, 2012, **48**, 4106–4108.

47 S. Evers and L. F. Nazar, *Chem. Commun.*, 2012, **48**, 1233–1235.

48 X. He, J. Ren, L. Wang, W. Pu, C. Jiang and C. Wan, *J. Power Sources*, 2009, **190**, 154–156.

49 G. Y. Zheng, Y. Yang, J. J. Cha and S. S. S. Y. Cui, *Nano Lett.*, 2011, **11**, 4462–4467.

50 W. Zheng, Y. W. Liu, X. G. Hu and C. F. Zhang, *Electrochim. Acta*, 2006, **51**, 1330–1335.

51 W. Ahn, K.-B. Kim, K.-N. Jung, K.-H. Shin and C.-S. Jin, *J. Power Sources*, 2012, **202**, 394–399.

52 L. X. Yuan, H. P. Yuan, X. P. Qiu, L. Q. Chen and W. T. Zhu, *J. Power Sources*, 2009, **189**, 1141–1146.

53 R. Demir-Cakan, M. Morcrette, F. Nouar, C. Davoisne, T. Devic, D. Gonbeau, R. Dominko, C. Serre, G. Ferrey and J.-M. Tarascon, *J. Am. Chem. Soc.*, 2011, **133**, 16154–16160.

54 J.-j. Chen, Q. Zhang, Y.-n. Shi, Y.-l. Qin, Y. Cao, M.-s. Zheng and Q.-f. Dong, *Phys. Chem. Chem. Phys.*, 2012, **14**, 5376–5382.

55 R. Elazari, G. Salitra, A. Garsuch, A. Panchenko and D. Aurbach, *Adv. Mater.*, 2011, **23**, 5641–5644.

56 L. Ji, M. Rao, S. Aloni, L. Wang, E. J. Cairns and Y. Zhang, *Energy Environ. Sci.*, 2011, **4**, 5053–5059.

57 L. Xiao, Y. Cao, J. Xiao, B. Schwenzer, M. H. Engelhard, L. V. Saraf, Z. Nie, G. J. Exarhos and J. Liu, *Adv. Mater.*, 2012, **24**, 1176–1181.

58 R. J. Chen, F. Wu, J. Z. Chen, S. X. Wu, L. Li, S. Chen and T. Zhao, *J. Phys. Chem. C*, 2011, **115**, 6057–6063.

59 N. Holten-Andersen, M. J. Harrington, H. Birkedal, B. P. Lee, P. B. Messersmith, K. Y. C. Lee and J. H. Waite, *Proc. Natl. Acad. Sci. U. S. A.*, 2011, **108**, 2651–2655.

60 M. D. Hager, P. Greil, C. Leyens, S. Van Der Zwaag and U. S. Schubert, *Adv. Mater.*, 2010, **22**, 5424–5430.

This journal is © The Royal Society of Chemistry 2013

Chem. Soc. Rev., 2013, **42**, 3018–3032 | **3031**

61 C. D. Dimitrakopoulos and P. R. L. Malenfant, *Adv. Mater.*, 2002, **14**, 99–117.

62 S. Günes, H. Neugebauer and N. S. Sariciftci, *Chem. Rev.*, 2007, **107**, 1324–1338.

63 J. L. Wang, J. Yang, J. Y. Xie and N. X. Xu, *Adv. Mater.*, 2002, **14**, 963–965.

64 J. Wang, J. Yang, C. Wan, K. Du, J. Xie and N. Xu, *Adv. Funct. Mater.*, 2003, **13**, 487–492.

65 X.-g. Yu, J.-y. Xie, J. Yang, H.-j. Huang, K. Wang and Z.-s. Wen, *J. Electroanal. Chem.*, 2004, **573**, 121–128.

66 X. Yu, J. Xie, Y. Li, H. Huang, C. Lai and K. Wang, *J. Power Sources*, 2005, **146**, 335–339.

67 A. Gorkovenko, T. A. Skotheim and Z.-S. Xu, *U.S. Patent*, 6878488, 2005.

68 M.-S. Song, S.-C. Han, H.-S. Kim, J.-H. Kim, K.-T. Kim, Y.-M. Kang, H.-J. Ahn, S. X. Dou and J.-Y. Lee, *J. Electrochem. Soc.*, 2004, **151**, A791–A795.

69 Y. J. Choi, B. S. Jung, D. J. Lee, J. H. Jeong, K. W. Kim, H. J. Ahn, K. K. Cho and H. B. Gu, *Phys. Scr.*, 2007, **T129**, 62–65.

70 X. Ji, S. Evers, R. Black and L. F. Nazar, *Nat. Commun.*, 2011, **2**, 325.

71 M. He, L.-X. Yuan, W.-X. Zhang, X.-L. Hu and Y.-H. Huang, *J. Phys. Chem. C*, 2011, **115**, 15703–15709.

72 J. Sun, Y. Huang, W. Wang, Z. Yu, A. Wang and K. Yuan, *Electrochim. Acta*, 2008, **53**, 7084–7088.

73 Y. Huang, J. Sun, W. Wang, Y. Wang, Z. Yu, H. Zhang, A. Wang and K. Yuan, *J. Electrochem. Soc.*, 2008, **155**, A764–A767.

74 Y. Wang and H. Zhou, *Energy Environ. Sci.*, 2011, **4**, 1704–1707.

75 N.-I. Kim, C.-B. Lee, J.-M. Seo, W.-J. Lee and Y.-B. Roh, *J. Power Sources*, 2004, **132**, 209–212.

76 H. Schneider, A. Garsuch, A. Panchenko, O. Gronwald, N. Janssen and P. Novak, *J. Power Sources*, 2012, **205**, 420–425.

77 Y. Jung and S. Kim, *Electrochem. Commun.*, 2007, **9**, 249–254.

78 X. Liang, Z. Wen, Y. Liu, M. Wu, J. Jin, H. Zhang and X. Wu, *J. Power Sources*, 2011, **196**, 9839–9843.

79 H. Wu, G. Chan, J. W. Choi, I. Ryu, Y. Yao, M. T. McDowell, S. W. Lee, A. Jackson, Y. Yang, L. Hu and Y. Cui, *Nat. Nanotechnol.*, 2012, **7**, 1–6.

80 Y. Yang, M. T. McDowell, A. Jackson, J. J. Cha, S. S. Hong and Y. Cui, *Nano Lett.*, 2010, **10**, 1486–1491.

81 M. N. Obrovac and J. R. Dahn, *Electrochem. Solid-State Lett.*, 2002, **5**, A70–A73.

82 T. Takeuchi, H. Sakaebe, H. Kageyama, H. Senoh, T. Sakai and K. Tatsumi, *J. Power Sources*, 2010, **195**, 2928–2934.

83 J. Kim, J. Hassoun, S. Panero, Y.-K. Sun and B. Scrosati, *Green*, 2011, **1**, 323–328.

84 M. Nagao, A. Hayashi and M. Tatsumisago, *J. Mater. Chem.*, 2012, **22**, 10015–10020.

85 J. Hassoun and B. Scrosati, *Angew. Chem., Int. Ed.*, 2010, **49**, 2371–2374.

86 Y. N. Zhou, C. L. Wu, H. Zhang, X. J. Wu and Z. W. Fu, *Electrochim. Acta*, 2007, **52**, 3130–3136.

87 A. Hayashi, R. Ohtsubo, T. Ohtomo, F. Mizuno and M. Tatsumisago, *J. Power Sources*, 2008, **183**, 422–426.

88 J. Gao, M. A. Lowe, Y. Kiya and H. D. Abruna, *J. Phys. Chem. C*, 2011, **115**, 25132–25137.

89 W. K. Wang, Y. Wang, Y. Q. Huang, C. J. Huang, Z. B. Yu, H. Zhang, A. B. Wang and K. G. Yuan, *J. Appl. Electrochem.*, 2010, **40**, 321–325.

90 D. R. Chang, S. H. Lee, S. W. Kim and H. T. Kim, *J. Power Sources*, 2002, **112**, 452–460.

91 J. H. Shin and E. J. Cairns, *J. Power Sources*, 2008, **177**, 537–545.

92 D. Aurbach, E. Pollak, R. Elazari, G. Salitra, C. S. Kelley and J. Affinito, *J. Electrochem. Soc.*, 2009, **156**, A694.

93 S. S. Zhang and J. A. Read, *J. Power Sources*, 2012, **200**, 77–82.

94 S. S. Zhang and D. T. Tran, *J. Power Sources*, 2012, **211**, 169–172.

95 J. H. Shin and E. J. Cairns, *J. Power Sources*, 2008, **177**, 537–545.

96 S.-E. Cheon, K.-S. Ko, J.-H. Cho, S.-W. Kim, E.-Y. Chin and H.-T. Kim, *J. Electrochem. Soc.*, 2003, **150**, A796–A805.

97 H. S. Ryu, Z. Guo, H. J. Ahn, G. B. Cho and H. Liu, *J. Power Sources*, 2009, **189**, 1179–1183.

98 L. Yuan, X. Qiu, L. Chen and W. Zhu, *J. Power Sources*, 2009, **189**, 127–132.

99 F. Wu, J. Chen, R. Chen, S. Wu, L. Li, S. Chen and T. Zhao, *J. Phys. Chem.*, 2011, **115**, 6057–6063.

100 J. Wang, J. Chen, K. Konstantinov, L. Zhao, S. H. Ng, G. X. Wang, Z. P. Guo and H. K. Liu, *Electrochim. Acta*, 2006, **51**, 4634–4638.

101 Y. Wang, Y. Huang, W. Wang, C. Huang, Z. Yu, H. Zhang, J. Sun, A. Wang and K. Yuan, *Electrochim. Acta*, 2009, **54**, 4062–4066.

102 Y. J. Choi, Y. D. Chung, C. Y. Baek, K. W. Kim, H. J. Ahn and J. H. Ahn, *J. Power Sources*, 2008, **184**, 548–552.

103 H. Ryu, H. Ahn, K. Kim, J. Ahn and J. Lee, *J. Power Sources*, 2006, **153**, 360–364.

104 S. S. Jeong, Y. Lim, Y. J. Choi, G. B. Cho, K. W. Kim, H. J. Ahn and K. K. Cho, *J. Power Sources*, 2007, **174**, 745–750.

105 J. Nelson, S. Misra, Y. Yang, A. Jackson, Y. Liu, H. Wang, H. Dai, J. C. Andrews, Y. Cui and M. F. Toney, *J. Am. Chem. Soc.*, 2012, **134**, 6337–6343.

106 Y. Liu, J. C. Andrews, J. Wang, F. Meirer, P. Zhu, Z. Wu and P. Pianetta, *Opt. Express*, 2011, **19**, 540–545.

107 J. C. Andrews, E. Almeida, M. C. H. Van Der Meulen, J. S. Alwood, C. Lee, Y. Liu, J. Chen, F. Meirer, M. Feser, J. Gelb, J. Rudati, A. Tkachuk, W. Yun and P. Pianetta, *Microsc. Microanal.*, 2010, **16**, 327–336.

108 H.-S. Ryu, H.-J. Ahn, K.-W. Kim, J.-H. Ahn, K.-K. Cho, T.-H. Nam, J.-U. Kim and G.-B. Cho, *J. Power Sources*, 2006, **163**, 201–206.

109 J. H. Shin and E. J. Cairns, *J. Electrochem. Soc.*, 2008, **155**, A368.

3032 | *Chem. Soc. Rev.*, 2013, **42**, 3018–3032

This journal is © The Royal Society of Chemistry 2013